Acta Mechanica Solida Sinica, Vol. 32, No. 5, October, 2019, 633–642 ISSN 1860-2134
https://doi.org/10.1007/s10338-019-00107-5

Finite Indentation of Pressurized Elastic Fluid Nanovesicles by a Rigid Cylindrical Indenter

Xingyi Tang[1] **Jianxiang Wang**[1,2] **Xin Yi**[1,3⋆]

([1] *Department of Mechanics and Engineering Science, College of Engineering, Peking University, Beijing 100871, China*)

([2] *CAPT, HEDPS and IFSA Collaborative Innovation Center of MoE, Peking University, Beijing 100871, China*)

([3] *Beijing Innovation Center for Engineering Science and Advanced Technology, Peking University, Beijing 100871, China*)

Received 24 February 2019; revision received 1 April 2019; Accepted 9 April 2019;
published online 19 June 2019

ABSTRACT Nanovesicles have been demonstrated to be the key agents in therapeutic encapsulations for drug delivery and diagnostic area, and the effectiveness and efficiency of these applications strongly depend on the mechanical properties of nanovesicles. Based on the Helfrich membrane theory, a theoretical investigation is conducted to explore the mechanical behaviors of pressurized elastic fluid nanovesicles during the indentation by a rigid cylindrical indenter. The effects of osmotic pressure, membrane bending rigidity, energy of adhesion between the vesicle and substrate on the mechanical responses of the vesicle to the indentation are analyzed. It is found that the osmotic pressure dominates the mechanical behaviors of strongly pressurized nanovesicles as well as the effective vesicle stiffness and Young's modulus. Our results may have important implications on regulating the mechanical behaviors of inter- and intracellular nanovesicles which are crucial for particle-based drug delivery systems.

KEY WORDS Nanovesicles, Indentation, Osmotic pressure, Young's modulus, Stiffness, Force-depth curves

1. Introduction

Nanovesicles, such as nanosized liposomes, extracellular vesicles, lysosomes, and endosomes, are ubiquitous in living cells and widely used as delivery vehicles in biomedical applications. From a mechanical point of view, a nanovesicle with a fluidic lipid membrane and a hollow interior compartment can be regarded as an elastic fluid thin structure, which could undergo large deformation upon small extent of external loading due to the fluidic and soft natures of the lipid membrane. Taking advantages of the tunable geometrical, mechanical, and physicochemical properties, nanovesicles not only play important functional roles in numerous cell activities including intercellular transport and communication [1, 2], cell uptake [3, 4], and pathogen infections [5], but also serve as a promising platform in drug delivery, biomedical diagnostics, and therapeutics [6–11]. So far, it has become widely recognized that the mechanical properties of nanoparticles play critical roles in some of the fields mentioned above, such as cell uptake, drug delivery, and cytotoxicity. For example, softer nanovesicles

⋆ Corresponding author. E-mail: xyi@pku.edu.cn

require more adhesion energy than stiffer ones to achieve a complete wrapping by the cell membrane [3, 4]. The cytoskeleton and actin networks approximated as elastic solid thin shells underneath the cell membranes are also expected to play important roles in regulating the cell uptake of nanovesicles [12, 13]. It has been demonstrated that the intracellular accumulation rate and distribution of nanoparticles exhibit stiffness-dependence [6, 14]. In addition, nanovesicles used as therapeutic encapsulations for drug delivery exhibited efficient accumulation and penetration in comparison with conventional solid micro-encapsulations [7]. Therefore, determination of the mechanical properties of nanovesicles is a crucial step in comprehending the diagnostic functions of nanovesicles and developing effective drug delivery strategies.

The techniques used for studying giant vesicles, such as micropipette aspiration and shape fluctuation analysis, involving and relying on optical imaging of shape fluctuations, were developed for large vesicles at microscale, and therefore, are less suitable for nanovesicles [15, 16]. Nanoscale indentations using the atomic force microscopy (AFM) have been employed in studying the apparent mechanical properties of nanovesicles, and demonstrated to be a valuable and sensitive approach [17–20]. However, the reported measurement results are inconsistent and exhibit large scatter, partly due to the fact that these nanoindentation analyses on the mechanical properties of nanovesicles were based on the classical continuum contact mechanics modeling such as the classical Hertz theory [21, 22], which are more suitable for elastic solid materials rather than elastic fluid structures such as nanovesicles. Other reasons complicating the modeling of nanovesicle indentation include the characterization of the largely deformed vesicle and the contact between the vesicle and the indenter tip as well as the contact between the vesicle and the substrate. A local point force was used in the existing literature to simplify the contact between the indenter tip and the vesicle, and the vesicle–substrate contact was ignored as a closed vesicle of a vertically symmetric configuration subject to a pair of contact forces upon the vesicle poles was adopted [20]. Such treatment could induce unphysical contact and geometrical conditions.

Here we develop a theoretical model to probe the mechanical behaviors of pressurized elastic fluid nanovesicles during the indentation by a rigid cylindrical indenter. Combing the angle-arclength parametrization with the interior-point optimization approach to characterize the vesicle deformation, we build a minimal model taking into account both small and large indentations with appropriate mechanical conditions and systematically analyze the effects of osmotic pressure, membrane bending rigidity, and energy of adhesion between the vesicle and the flat substrate on the indentation force-depth curves. Moreover, the effective stiffness and Young's modulus of the vesicle are determined. Our results shed light on the mechanical behaviors of elastic fluid vesicles and may have important implications in therapeutic encapsulations for drug delivery and diagnostic area.

2. Modeling and Method

In the adopted cylindrical coordinate (r, θ, z), we consider an initial spherical nanovesicle undergoing an axisymmetric deformation upon indentation by a rigid cylindrical indenter (Fig. 1). The indentation depth Δh is defined as the distance between the apex of the indenter tip and the north pole of the vesicle before indentation (the dashed line in Fig. 1). In the modeling, the vesicle is divided into three regions: (1) the upper region of the contact between the indenter tip and the vesicle, (2) the middle free region, and (3) the lower region of the contact between the vesicle and the substrate. Quantities associated with these three regions are labeled by subscripts 1, 2, and 3, respectively.

In our model, the vesicle area A is assumed to be constant as $A = 4\pi R^2$, with R the effective radius of the vesicle. By adopting the Canham–Helfrich membrane theory, the total free energy of the system at a certain indentation depth Δh is given as [23]

$$E_{\text{tot}} = 2\kappa \int M_1^2 \mathrm{d}A_1 + 2\kappa \int M_2^2 \mathrm{d}A_2 - \Delta p(V - V_0) - \gamma A_3 \tag{1}$$

where κ, M_i, and A_i $(i = 1, 2)$ are the bending rigidity, mean curvature and area element of the vesicle membrane, respectively; Δp is the constant osmotic pressure or the pressure difference between the interior and exterior of the vesicle; $V_0 (= 4\pi R^3/3)$ and V are the volumes of the original and deformed vesicle, respectively; A_3 is the area of the vesicle–substrate contact region; and γ is the adhesion energy. The fixed total surface area requires $A = A_1 + A_2 + A_3$. Zero spontaneous curvature is assumed. In

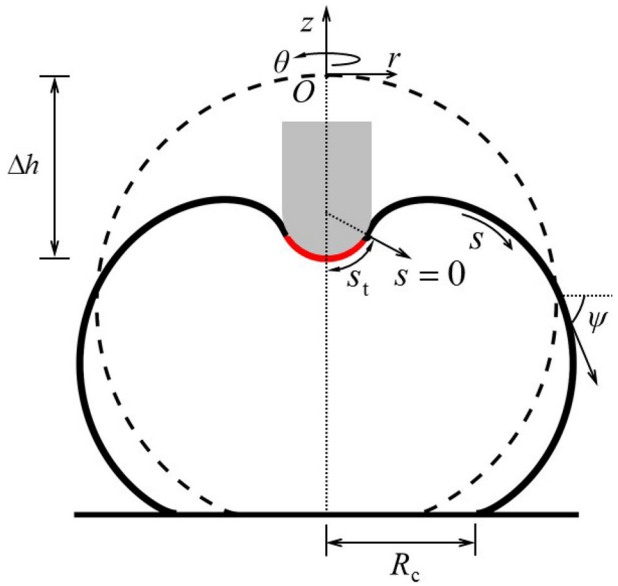

Fig. 1. Schematic illustration of the indentation of a pressurized nanovesicle by a rigid cylindrical indenter (the gray region). The red curve depicts the upper region of the contact between the indenter tip and the vesicle, and the total arclength of this region is s_t. The arclength s of the free vesicle region is measured along the meridian of the nanovesicle, originating from the upper contact edge and ending at the lower contact edge, whose r-coordinate is R_c. The total arclength of the free vesicle region is I_2. The tangent angle ψ is positive as it is measured counterclockwise from the positive r-axis. (Color figure online)

this work, we focus on the case that the adhesive interaction between the indenter tip and the vesicle is negligible.

The cylindrical indenter has a semi-spherical cap of radius R_t at the apex. From simple geometrical considerations, we can determine the (r, z) coordinates of the upper contact edge as $(r_\mathrm{c}, z_\mathrm{c})$

$$\begin{cases} r_\mathrm{c} = R_\mathrm{t} \sin \frac{s_\mathrm{t}}{R_\mathrm{t}}, \quad z_\mathrm{c} = R_\mathrm{t} \left(1 - \cos \frac{s_\mathrm{t}}{R_\mathrm{t}}\right) - \Delta h & \left(s_\mathrm{t} \le \frac{\pi R_\mathrm{t}}{2}\right) \\ r_\mathrm{c} = R_\mathrm{t}, \quad z_\mathrm{c} = s_\mathrm{t} - R_\mathrm{t} \left(\frac{\pi}{2} - 1\right) - \Delta h & \left(s_\mathrm{t} > \frac{\pi R_\mathrm{t}}{2}\right) \end{cases} \tag{2}$$

where s_t is the total arclength of the upper contact region. The tangent angle ψ_c at the upper contact edge is $\psi_\mathrm{c} = s_\mathrm{t}/R_\mathrm{t}$ at $s_\mathrm{t} \le \pi R_\mathrm{t}/2$ or $\psi_\mathrm{c} = \pi/2$ at $s_\mathrm{t} > \pi R_\mathrm{t}/2$.

The volume V_1 of the tip covered by the upper contact region is

$$V_1 = \begin{cases} \frac{4}{3}\pi R_\mathrm{t}^3 \left(2 + \cos \frac{s_\mathrm{t}}{R_\mathrm{t}}\right) \sin^4 \frac{s_\mathrm{t}}{2R_\mathrm{t}} & \left(s_\mathrm{t} \le \frac{\pi R_\mathrm{t}}{2}\right) \\ \pi R_\mathrm{t}^3 \left(\frac{s_\mathrm{t}}{R_\mathrm{t}} + \frac{2}{3} - \frac{\pi}{2}\right) & \left(s_\mathrm{t} > \frac{\pi R_\mathrm{t}}{2}\right) \end{cases} \tag{3}$$

and the area A_1 of the membrane in the upper contact region is

$$A_1 = \begin{cases} 2\pi R_\mathrm{t}^2 \left(1 - \cos \frac{s_\mathrm{t}}{R_\mathrm{t}}\right) & \left(s_\mathrm{t} \le \frac{\pi R_\mathrm{t}}{2}\right) \\ \pi R_\mathrm{t}^2 \left(\frac{2s_\mathrm{t}}{R_\mathrm{t}} + 2 - \pi\right) & \left(s_\mathrm{t} > \frac{\pi R_\mathrm{t}}{2}\right) \end{cases} \tag{4}$$

The bending energy E_1 of the vesicle membrane in the upper contact region is determined as

$$E_1 = \begin{cases} 4\pi\kappa \left(1 - \cos \frac{s_\mathrm{t}}{R_\mathrm{t}}\right) & \left(s_\mathrm{t} \le \frac{\pi R_\mathrm{t}}{2}\right) \\ \pi\kappa \left(4 - \frac{\pi}{2} + \frac{s_\mathrm{t}}{R_\mathrm{t}}\right) & \left(s_\mathrm{t} > \frac{\pi R_\mathrm{t}}{2}\right) \end{cases} \tag{5}$$

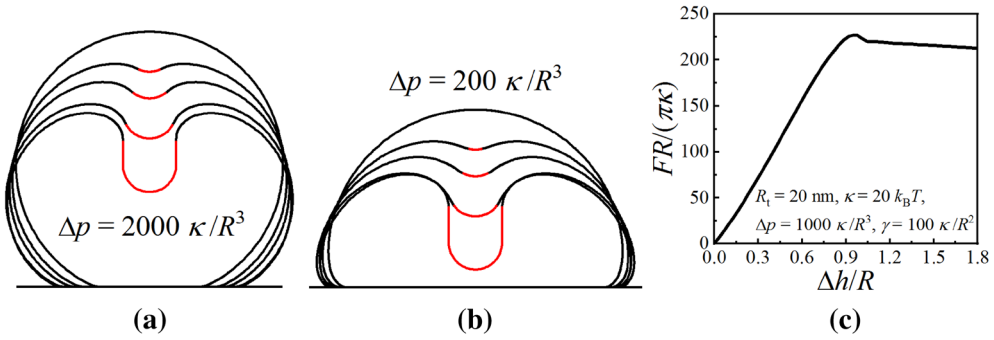

Fig. 2. Equilibrium configurations of pressurized nanovesicles for different indentation depths $\Delta h/R = 0$, 0.3, 0.5, 0.8, and 1.2 at osmotic pressure $\Delta p = 2000\kappa/R^3$ (**a**) and $200\kappa/R^3$ (**b**). The red curves represent the vesicle–indenter contact region. (**c**) The normalized indentation force as a function of the normalized indentation depth. Here we take $R = 100$ nm, $R_t = 20$ nm, $\kappa = 20\,k_BT$, and $\gamma = 100\kappa/R^2$. (Color figure online)

In the free vesicle region, the vesicle configuration is characterized by the tangent angle $\psi(s)$, with s the arclength of the free region. Therefore, the mean curvature is $M_2 = (\sin\psi/r + \mathrm{d}\psi/\mathrm{d}s)/2$. The bending energy E_2 of the free region is

$$E_2 = 2\kappa \int M_2^2 \mathrm{d}A_2 = \pi\kappa \int_0^{l_2} \left(\frac{\mathrm{d}\psi}{\mathrm{d}s} + \frac{\sin\psi}{r}\right)^2 r\mathrm{d}s \tag{6}$$

where l_2 is the undetermined total arclength of the free region. The area A_2 of the free region is $A_2 = 2\pi \int_0^{l_2} r\mathrm{d}s$. The volume of the deformed vesicle is $V = -V_1 - \pi \int_0^{l_2} r^2 \sin\psi \mathrm{d}s$.

In the lower contact region, the flat membrane has zero bending energy and the contact area is $A_3 = \pi R_c^2$, with $R_c = r_c + \int_0^{l_2} \cos\psi \mathrm{d}s$ the radius of contact between the vesicle and the substrate. At the lower contact edge ($s = l_2$), we have $\psi = -\pi$.

The total system energy E_{tot} is characterized as a function of tangent angle ψ, which is approximated by a cubic B-spline curve as $\psi(t) = \sum_{i=0}^{n} a_i N_i(t)$. Here $t = s/l_2$ is a new variable introduced to normalize the unknown total arclength l_2 of the free region to 1, so that $t = 0$ and 1 at the upper and lower contact edges, respectively [24]. Here the control points a_i are the coefficients of the basic function $N_i(t)$, which are defined on a nonuniform knot vector $\{\eta_0, \eta_1, \ldots, \eta_{n+4}\}$ ($\eta \in [0, 1]$) with $\eta_j = 0 (j = 0, \ldots, 3)$ and $\eta_j = 1 (j = n+1, \ldots, n+4)$. In our calculation, we choose $n = 82$.

The interior-point optimization approach taking into account nonlinear constraints is employed to numerically minimize E_{tot} at a given indentation depth Δh; the fixed vesicle area A serves as an equality constraint; and inequality constraints are introduced to prevent penetration between the vesicle and the cylindrical indenter [25, 26]. The first and second derivatives of E_{tot} with respect to the undetermined parameters a_i, s_t and l_2 are required. Once the minimum energy is obtained, the indentation force $F = \mathrm{d}E_{\mathrm{tot}}/\mathrm{d}(\Delta h)$ can be determined. Existing theoretical studies on the adhesion of vesicles to a rigid flat surface [27] serve as good benchmarks for the validation of our numerical approach. We perform a series of calculations at $\Delta h = 0$ and certain sets of Δp and γ, and successfully repeat the reported results in [27]. Detailed comparisons are not shown here to stay focused on the vesicle indentation.

3. Results and Discussion

Figure 2a, b shows the equilibrium configurations of pressurized nanovesicles of radius $R = 100$ nm at different osmotic pressures Δp and indentation depths $\Delta h/R = 0$, 0.3, 0.5, 0.8 and 1.2. As the indentation depth Δh increases, the areas of the upper and lower contact regions increase. Moreover, at large $\Delta h/R$, a membrane nanotube is formed. This is consistent with the recent experimental observation that an inward lipid membrane nanotube could be induced in a vesicle by pressing a trapped bead [28]. The force–depth curve in Fig. 2c shows that the indentation force F increases almost linearly with Δh, gradually deviates from that approximately linear relationship, rises to a

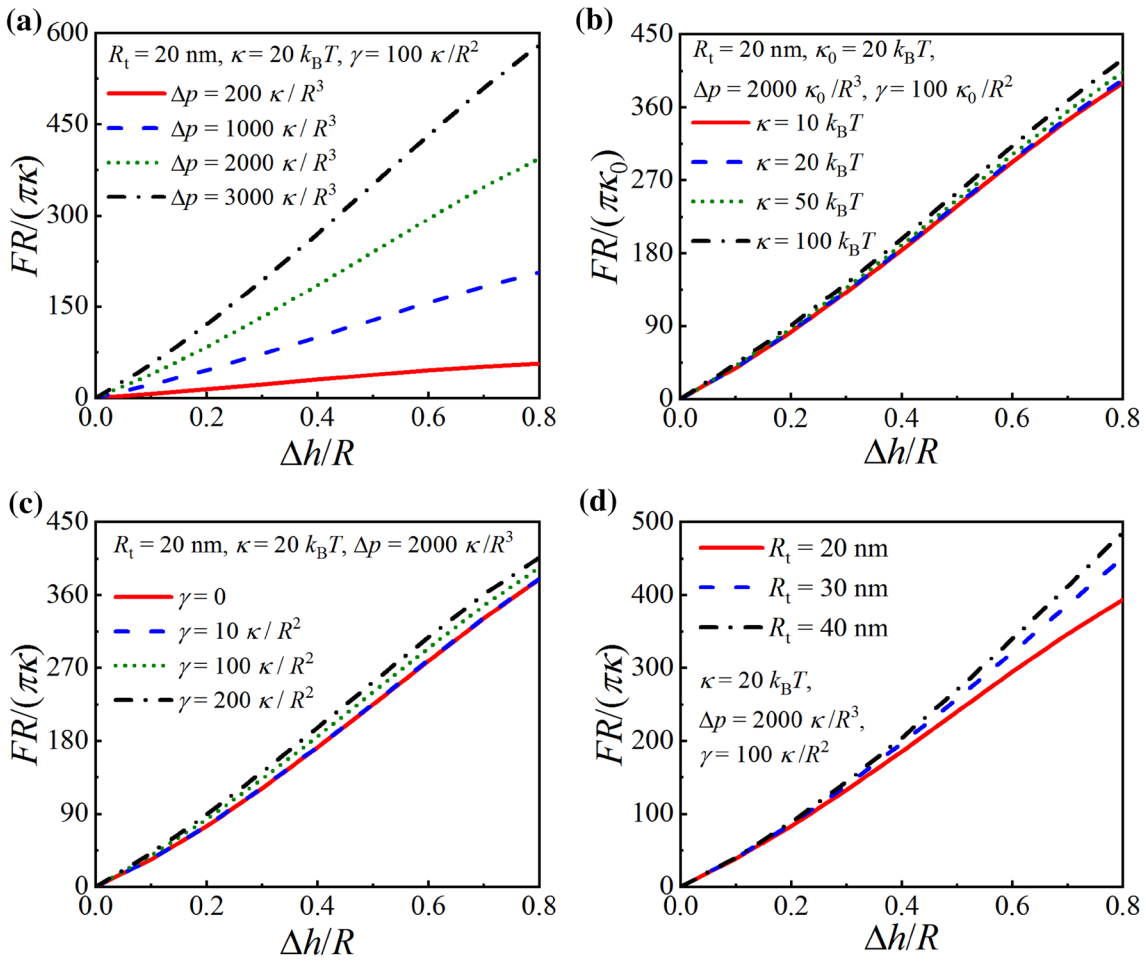

Fig. 3. Effects of the osmotic pressure Δp (**a**), membrane bending rigidity κ (**b**), adhesion energy γ (**c**), and indenter tip radius R_t (**d**) on the indentation force-depth curves

peak value f_{max}, and then decreases upon the formation of an inward tubular membrane protrusion. Upon inward tubulation, the indentation force F almost saturates and is insensitive to $\Delta h/R$. Similar features have been observed in the cases of packing of nanorods with finite diameters in vesicles [25, 29] and in the cylindrical indentation of a hyperelastic membrane [30]. The inward tubulation here can be regarded as a type of tubular morphological transition of vesicles. Another similar type of tubular transition is the enforced detachment of an adhesive vesicle from the substrate, which is accompanied with a sharp drop of the external pulling force [31].

Here we focus on the mechanical behaviors of the vesicle and assume that both the indenter and the vesicle membrane remain intact. In the case of a rigid nanoindenter of strong surface hydrophobicity, e.g., an indenter coated with pristine graphene, there exists strong hydrophobic interaction between the indenter surface and the tails of lipid molecules composing the vesicle membrane, and upon persistent indentation, phospholipids might be extracted from the vesicle membrane onto the indenter surface to maximize the hydrophobic interaction [9, 32].

To systematically explore the mechanical behaviors of the pressurized nanovesicle subject to indentation, we investigate the F-Δh relation at different values of osmotic pressure Δp, membrane bending rigidity κ, adhesion energy γ and indenter radius R_t (Fig. 3). Figure 3 shows that the slopes of the force-displacement curves increase as Δp, κ, γ, and R_t increase. Moreover, the osmotic pressure Δp dominates the mechanical responses of the nanovesicle to indentation in comparison with κ, γ, and R_t (Fig. 3).

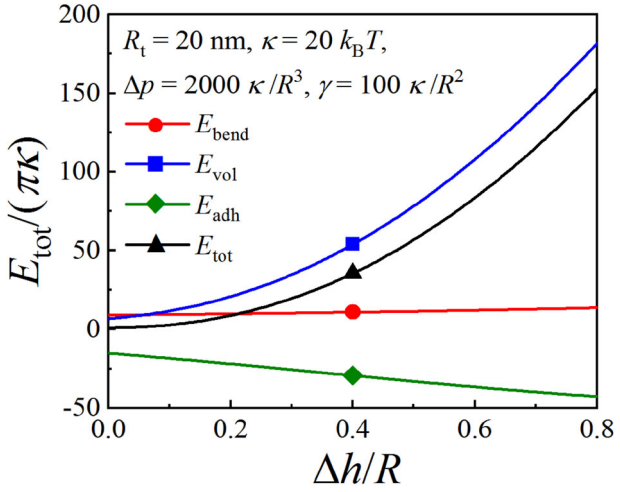

Fig. 4. Variations of the total system energy $E_{\rm tot}$ and its three components $E_{\rm bend}$, $E_{\rm vol}$ and $E_{\rm adh}$ as functions of the indentation depth Δh. Here the bending energy $E_{\rm bend}$ is defined as $E_{\rm bend} = 2\kappa \int M_1^2 {\rm d}A_1 + 2\kappa \int M_2^2 {\rm d}A_2$, the work done by the osmotic pressure is $E_{\rm vol} = -\Delta p(V - V_0)$, and the adhesion energy is $E_{\rm adh} = -\gamma A_3$

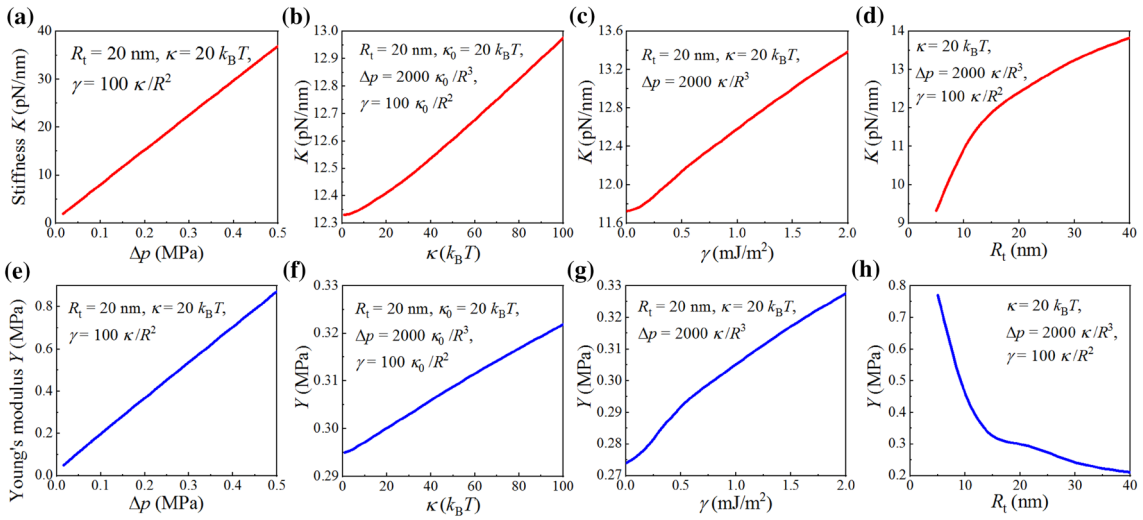

Fig. 5. Effects of the osmotic pressure Δp (**a**,**e**), membrane bending rigidity κ (**b**,**f**), adhesion energy γ (**c**,**g**), and indenter tip radius $R_{\rm t}$ (**d**,**h**) on the effective stiffness K and Young's modulus Y of the nanovesicles. The nanovesicle radius is taken as $R = 100$ nm

Figure 4 shows variations of the total energy $E_{\rm tot}$ and its three components $E_{\rm bend}$, $E_{\rm vol}$ and $E_{\rm adh}$ as functions of Δh at $\Delta p = 2000\kappa/R^3$. Other parameters have the same values as those in Fig. 2. It is demonstrated that $E_{\rm vol}$ plays a dominant role among these three components, while $E_{\rm bend}$ has a minor effect on the nanovesicle response to the indentation. These conclusions are consistent with the force-depth curves in Fig. 3, which show that the indentation force F strongly depends on osmotic pressure Δp, but is relatively insensitive to the membrane bending rigidity κ.

The effective vesicle stiffness of the nanovesicle can be determined as the slope of the force-depth curve $K = {\rm d}F/{\rm d}(\Delta h)$. Here we linearize the F-Δh curves in the range of $\Delta h/R$ from 0.2 to 0.3, and define the corresponding slope as the effective vesicle stiffness K. Figure 5a shows a linear proportionality between the osmotic pressure Δp and the effective vesicle stiffness K or ${\rm d}F/{\rm d}(\Delta h)$ at sufficiently large Δh. A similar linear relation of ${\rm d}F/{\rm d}(\Delta h)$-$\Delta p$ has been reported theoretically for a pressurized linear elastic solid thin shell upon indentation [33]. The K-κ and K-γ curves exhibit approximately linear relations at relatively large κ and γ (Fig. 5b, c). One can find that the effects of κ and γ on K

are minor compared with that of Δp. The dominance of K associated with Δp is consistent with our analysis in Figs. 3 and 4. In addition, the effective vesicle stiffness K exhibits size-dependence on the indenter radius R_t (Fig. 5d). A larger indenter induces a higher stiffness.

Besides the effective stiffness K, the Young's modulus Y serves as another widely used parameter to characterize the apparent rigidity of target materials or structures, which is usually estimated based on the continuum contact mechanics theory [21, 22]. The classical Hertz theory, only suitable for the shallow indentation, does not apply to soft matters such as elastic fluid vesicles which could undergo finite deformation at a small indentation force. Here we employ the Sneddon theory [34, 35] to achieve a more appropriate estimation on the Young's modulus Y of vesicle, which releases the enforcement of small deformation required by the classical Hertz theory. It is worth noting that the Sneddon theory was originally proposed for a punch of arbitrary profile using the linear elastic contact theory at small deformation [34], and later it has been shown that the Sneddon's solution is applicable for interpreting the indentation of nonlinear elastic materials when the ratio between the indentation depth and indenter size is not significantly large [36].

According to the Sneddon theory [34, 35], the relation between the indentation force F and the Young's modulus Y is

$$F = \frac{Y}{1-\nu^2}\left[\frac{R_t^2 + a^2}{2}\ln\left(\frac{R_t + a}{R_t - a}\right) - aR_t\right] \tag{7}$$

where a is the apparent contact radius given by $\Delta h = (a/2)\ln[(R_t + a)/(R_t - a)]$. Assuming the Poisson ratio $\nu = 0.5$, we can determine the Young's modulus Y at a given indentation depth Δh. In our calculation, we take Y at $\Delta h/R = 0.3$ as the effective Young's modulus of the vesicle.

The dependence of the effective Young's modulus Y on the osmotic pressure Δp, membrane bending rigidity κ, and adhesion energy γ, as shown in Fig. 5e–g, is analogous to that of K in Fig. 5a–c. Note that the effective Young's modulus Y decreases as the indenter size R_t increases (Fig. 5h), while the effective vesicle stiffness K increases as R_t increases (Fig. 5d). The contrast of the effects of R_t on Y and K is consistent with the previous experiments on the indentation of tomato mesocarp cells [37]. This counterintuitive phenomenon could be explained as follows. As R_t increases, the indenter tip is more flattened locally and F at the same Δh becomes larger, which leads to an increasing vesicle stiffness K. According to the contact mechanics theory including the Sneddon theory, Y is proportional to F but inversely proportional to R_t. A competition between the force F and indenter radius R_t leads to a decreasing Young's modulus Y as R_t increases.

The precise identification of the initial contact point is critical for the accurate analysis of the force-depth curves and determination of the sample stiffness or modulus. In theoretical studies, the point of initial contact between the indenter tip and the sample is known a priori at the north pole of the vesicle before indentation ($\Delta h = 0$). In experimental studies, the determination of the initial contact point is not as straightforward as in theoretical studies. Based on sequential search algorithms and fitting with appropriate contact mechanics model, different automated and high-throughput approaches have been proposed to experimentally locate the point of initial contact between the indenter tip and the sample [38–41].

In practice, extracting the mechanical properties of samples from the measured force-depth curves involves inverse analysis and optimization with certain techniques such as dimensional analysis and iterative finite element analysis [42–46]. The central concerns in inverse analysis are the existence, uniqueness and stability of the solutions of the inverse problem [42, 43], among which the uniqueness and stability are more critical from an engineering point of view. Depending on the range of the mechanical properties of sample materials, the indenter size and shape, and the number of force-depth curves might be involved, and the systematic inverse analysis could be significantly challenging. The inverse analysis of nanovesicle indentation experiments certainly require further investigation in the future.

Theoretical models in the previous literature approximate the free region of the vesicle as a spherical cap under the condition of strong adhesive interaction between the vesicle and the substrate [47, 48]. To simplify the modeling of the contact between the indenter and the vesicle, a local point loading has been applied [20]. However, this approximation limits the modeling to the case of a small indenter in comparison with the size of the vesicle. In contrast to these models, using the angle-arclength

parametrization based on the B-spline curve, our model could accurately describe the vesicle deformation at deep and shallow indentations and integrate the precise boundary conditions at the upper and lower contact edges.

In this work, we focus on the indentation of the nanovesicle enclosed merely by a fluid membrane. For cells or engineered vesicles with actin cortex or protein network underlying the lipid bilayer membrane, a precise description of the mechanical response to indentation or other external stimuli requires a more sophisticated model incorporating the coupling of the Eulerian description of the fluid lipid membranes and the Lagrangian description of the underlying solid thin structures. A thorough and detailed theoretical analysis is deserved in the future.

4. Conclusions

A theoretical study has been performed to probe the indentation of pressurized nanovesicles, considering the effects of osmotic pressure, membrane bending rigidity, adhesive interaction between the vesicle and the substrate, and indenter tip size. The indentation force-depth curves at different values of osmotic pressure Δp, membrane bending rigidity κ, work of adhesion γ, and indenter tip radius R_{t} are obtained, and the effective vesicle stiffness and Young's modulus are determined. It is found that larger Δp, κ, and γ induce larger vesicle stiffness and Young's modulus. Moreover, the osmotic pressure dominates the effective stiffness and Young's modulus of the pressurized nanovesicle. Our results indicate that the osmotic pressure is a crucial factor to regulate the mechanical behaviors of inter- and intracellular nanovesicles, which has important implications in the fields of cell diagnostics and drug delivery.

Acknowledgements. Financial support for this work was provided by the National Natural Science Foundation of China (Grant Nos. 11872005 and 11521202).

References

[1] Colombo M, Raposo G, Théry C. Biogenesis, secretion, and intercellular interactions of exosomes and other extracellular vesicles. Annu Rev Cell Dev Biol. 2014;30(1):255–89.
[2] Regev-Rudzki N, Wilson DW, Carvalho TG, Sisquella X, Coleman BM, Rug M, et al. Cell-cell communication between malaria-infected red blood cells via exosome-like vesicles. Cell. 2013;153(5):1120–33.
[3] Yi X, Shi X, Gao H. Cellular uptake of elastic nanoparticles. Phys Rev Lett. 2011;107(9):098101.
[4] Sun J, Zhang L, Wang J, Feng Q, Liu D, Yin Q, Xu D, Wei Y, Ding B, Shi X, Jiang X. Tunable rigidity of (polymeric core)-(lipid shell) nanoparticles for regulated cellular uptake. Adv Mater. 2015;27(8):1402–7.
[5] Zhang W, Jiang X, Bao J, Wang Y, Liu H, Tang L. Exosomes in pathogen infections: a bridge to deliver molecules and link functions. Front Immunol. 2018;9:90.
[6] Anselmo AC, Mitragotri S. Impact of particle elasticity on particle-based drug delivery systems. Adv Drug Deliv Rev. 2017;108:51–67.
[7] Wang AZ, Langer R, Farokhzad OC. Nanoparticle delivery of cancer drugs. Annu Rev Med. 2012;63(1):185–98.
[8] Merkel TJ, Jones SW, Herlihy KP, Kersey FR, Shields AR, Napier M, et al. Using mechanobiological mimicry of red blood cells to extend circulation times of hydrogel microparticles. Proc Natl Acad Sci USA. 2011;108(2):586–91.
[9] Zhu W, von dem Bussche A, Yi X, Qiu Y, Wang Z, Weston P, Hurt RH, Kane AB, Gao H. Nanomechanical mechanism for lipid bilayer damage induced by carbon nanotubes confined in intracellular vesicles. Proc Natl Acad Sci USA. 2016;113(44):12374–9.
[10] Yu M, et al. Rapid transport of deformation-tuned nanoparticles across biological hydrogels and cellular barriers. Nat Commun. 2018;9:2607.
[11] Yu M, et al. Temperature- and rigidity-mediated rapid transport of lipid nanovesicles in hydrogels. Proc Natl Acad Sci USA. 2019;116(12):5362–9.
[12] Li L, Liu X, Zhou Y, Wang J. On resistance to virus entry into host cells. Biophys J. 2012;102(9):2230–3.
[13] Wang J, Li L. Coupled elasticity-diffusion model for the effects of cytoskeleton deformation on cellular uptake of cylindrical nanoparticles. J R Soc Interface. 2015;12(102):20141023.
[14] Anselmo AC, Zhang M, Kumar S, Vogus DR, Menegatti S, Helgeson ME, Mitragotri S. Elasticity of nanoparticles influences their blood circulation, phagocytosis, endocytosis, and targeting. ACS Nano. 2015;9(3):3169–77.
[15] Dimova R. Recent developments in the field of bending rigidity measurements on membranes. Adv Colloid Interface Sci. 2014;208:225–34.

[16] Bassereau P, Sorre B, Lévy A. Bending lipid membranes: experiments after W. Helfrich's model. Adv Colloid Interface Sci. 2014;208:47–57.
[17] Li S, Eghiaian F, Sieben C, Herrmann A, Schaap IAT. Bending and puncturing the influenza lipid envelope. Biophys J. 2011;100(3):637–45.
[18] Calò A, Reguera D, Oncins G, Persuy MA, Sanz G, Lobasso S, Corcelli A, Pajot-Augy E, Gomila G. Force measurements on natural membrane nanovesicles reveal a composition-independent, high Young's modulus. Nanoscale. 2014;6(4):2275–85.
[19] Takechi-Haraya Y, Sakai-Kato K, Abe Y, Kawanishi T, Okuda H, Goda Y. Observation of liposomes of differing lipid composition in aqueous medium by means of atomic force microscopy. J Electron Microsc. 2016;65(4):383–9.
[20] Vorselen D, MacKintosh FC, Roos WH, Wuite GJL. Competition between bending and internal pressure governs the mechanics of fluid nanovesicles. ACS Nano. 2017;11(3):2628–36.
[21] Johnson KL. Contact mechanics. Cambridge: Cambridge University Press; 1985.
[22] Maugis D. Contact, adhesion and rupture of elastic solids. Berlin: Springer; 2000.
[23] Helfrich W. Elastic properties of lipid bilayers: theory and possible experiments. Z Naturforsch C. 1973;28(11):693–703.
[24] Jiang HY, Huber G, Pelcovits RA, Powers TR. Vesicle shape, molecular tilt, and the suppression of necks. Phys Rev E. 2007;76(3):031908.
[25] Yi X, Zou G, Gao H. Mechanics of cellular packing of nanorods with finite and non-uniform diameters. Nanoscale. 2018;10(29):14090–9.
[26] Wu Z, Yuan H, Zhang X, Yi X. Sidewall contact regulating the nanorod packing inside vesicles with relative volumes. Soft Matter. 2019;15(12):2552–9.
[27] Seifert U, Lipowsky R. Adhesion of vesicles. Phys Rev A. 1990;42(8):4768–71.
[28] Dasgupta R, Dimova R. Inward and outward membrane tubes pulled from giant vesicles. J Phys D Appl Phys. 2014;47(28):282001.
[29] Zou G, Yi X, Zhu W, Gao H. Packing of flexible nanofibers in vesicles. Extrem Mech Lett. 2018;19:20–6.
[30] Liu J, Chen Z, Liang X, Huang X, Mao G, Hong W, Yu H, Qu S. Puncture mechanics of soft elastomeric membrane with large deformation by rigid cylindrical indenter. J Mech Phys Solids. 2018;112:458–71.
[31] Shi W, Feng XQ, Gao H. Two-dimensional model of vesicle adhesion on curved substrates. Acta Mech Sin. 2006;22(6):529–35.
[32] Tu Y, et al. Destructive extraction of phospholipids from *Escherichiacoli* membranes by graphene nanosheets. Nat Nanotechnol. 2013;8(8):594–601.
[33] Vella D, Ajdari A, Vaziri A, Boudaoud A. The indentation of pressurized elastic shells: from polymeric capsules to yeast cells. J R Soc Interface. 2012;9(68):448–55.
[34] Sneddon IN. The relation between load and penetration in the axisymmetric Boussinesq problem for a punch of arbitrary profile. Int J Eng Sci. 1965;3(1):47–57.
[35] Cappella B, Dietler G. Force-distance curves by atomic force microscopy. Surf Sci Rep. 1999;34(1):1–104.
[36] Zhang M-G, Chen J, Feng X-Q, Cao Y. On the applicability of Sneddon's solution for interpreting the indentation of nonlinear elastic biopolymers. J App Mech. 2014;81(9):091011.
[37] Zdunek A, Kurenda A. Determination of the elastic properties of tomato fruit cells with an atomic force microscope. Sensors. 2013;13(9):12175–91.
[38] Lin DC, Dimitriadis EK, Horkay F. Robust strategies for automated AFM force curve analysis–I. Non-adhesive indentation of soft, inhomogeneous materials. J Biomech Eng. 2007;129(3):430–40.
[39] Benítez R, Moreno-Flores S, Bolós VJ, Toca-Herrera JL. A new automatic contact point detection algorithm for AFM force curves. Microsc Res Tech. 2013;76(8):870–6.
[40] Hermanowicz P, Sarna M, Burda K, Gabrys H. AtomicJ: an open source software for analysis of force curves. Rev Sci Instrum. 2014;85(6):063703.
[41] Gavara N. Combined strategies for optimal detection of the contact point in AFM force-indentation curves obtained on thin samples and adherent cells. Sci Rep. 2016;6:21267.
[42] Cao YP, Lu J. Depth-sensing instrumented indentation with dual sharp indenters: stability analysis and corresponding regularization schemes. Acta Mater. 2004;52(5):1143–53.
[43] Cao YP, Lu J. A new method to extract the plastic properties of metal materials from an instrumented spherical indentation loading curve. Acta Mater. 2004;52(13):4023–32.
[44] Cheng Y-T, Cheng C-M. Can stress-strain relationships be obtained from indentation curves using conical and pyramidal indenters? J Mater Res. 1999;14(9):3493–6.
[45] Cheng Y-T, Cheng C-M. Scaling, dimensional analysis, and indentation measurements. Mater Sci Eng R. 2004;44(4–5):91–149.

[46] Chen X, Ogasawara N, Zhao M, Chiba N. On the uniqueness of measuring elastoplastic properties from indentation: the indistinguishable mystical materials. J Mech Phys Solids. 2007;55(8):1618–60.
[47] Schäfer E, Vache M, Kliesch TT, Janshoff A. Mechanical response of adherent giant liposomes to indentation with a conical AFM-tip. Soft Matter. 2015;11(22):4487–95.
[48] Sen S, Subramanian S, Discher DE. Indentation and adhesive probing of a cell membrane with AFM: theoretical model and experiments. Biophys J. 2005;89(5):3203–13.